Draft version September 10, 2020
Preprint typeset using LaTeX style emulateapj v. 01/23/15

LOW ENERGY MEASUREMENT OF THE ^{96}ZR$(\alpha, N)^{99}$MO REACTION CROSS SECTION AND ITS IMPACT ON WEAK R-PROCESS NUCLEOSYNTHESIS

G. G. Kiss
Institute for Nuclear Research (ATOMKI), H-4026 Debrecen, Bem tér 18/c, Hungary

T. N. Szegedi
Institute for Nuclear Research (ATOMKI), H-4026 Debrecen, Bem tér 18/c, Hungary
University of Debrecen, H-4001 Debrecen, Egyetem tér 1, Hungary

P. Mohr
Institute for Nuclear Research (ATOMKI), H-4026 Debrecen, Bem tér 18/c, Hungary

M. Jacobi
Institut für Kernphysik, Technische Universität Darmstadt, Schlossgartenstr. 2, D-64289 Darmstadt, Germany

Gy. Gyürky
Institute for Nuclear Research (ATOMKI), H-4026 Debrecen, Bem tér 18/c, Hungary

R. Huszánk
Institute for Nuclear Research (ATOMKI), H-4026 Debrecen, Bem tér 18/c, Hungary

A. Arcones
Institut für Kernphysik, Technische Universität Darmstadt, Schlossgartenstr. 2, D-64289 Darmstadt, Germany
GSI Helmholtzzentrum fr Schwerionenforschung GmbH, Planckstr. 1, D-64291 Darmstadt, Germany
Helmholtz Forschungsakademie Hessen für FAIR, GSI Helmholtzzentrum fr Schwerionenforschung, 64291 Darmstadt, Germany

Draft version September 10, 2020

ABSTRACT

Lighter heavy elements beyond iron and up to around silver can form in neutrino-driven ejecta in core-collapse supernovae and neutron star mergers. Slightly neutron-rich conditions favour a weak r-process that follows a path close to stability. Therefore, the beta decays are slow compared to the expansion time scales, and (α,n) reactions become critical to move matter towards heavier nuclei. The rates of these reactions are calculated with the statistical model and their main uncertainty, at energies relevant for the weak r-process, is the α+nucleus optical potential. There are several sets of parameters to calculate the α+nucleus optical potential leading to large deviations for the reaction rates, exceeding even one order of magnitude. Recently the ^{96}Zr(α,n)^{99}Mo reaction has been identified as a key reaction that impacts the production of elements from Ru to Cd. Here, we present the first cross section measurement of this reaction at energies (6.22 MeV $\leq$ E$_{\rm c.m.}$ $\leq$ 12.47 MeV) relevant for the weak r-process. The new data provide a stringent test of various model predictions which is necessary to improve the precision of the weak r-process network calculations. The strongly reduced reaction rate uncertainty leads to very well-constrained nucleosynthesis yields for $Z = 44-48$ isotopes under different neutrino-driven wind conditions.

Subject headings: nucleosynthesis, weak r-process, cross section measurement, optical model, statistical model

1. INTRODUCTION

Half of the stable isotopes heavier than iron are produced by the rapid neutron capture process (r-process) when neutron captures are faster than beta decays. This process requires extreme neutron densities and explosive environments, therefore the two favourite candidates are: core-collapse supernovae, where neutron stars are born, and neutron star mergers. After a successful core-collapse supernova, there is a neutrino-driven wind consisting of matter ejected by neutrinos emitted from the hot proto-neutron star. For many years, this was the preferred scenario for the r-process, even if the conditions were only slightly neutron rich or proton rich and thus not enough for the r-process (for a review see Arcones & Thielemann (2013) and reference therein). In contrast, the r-process has been observed in neutron star mergers. After the gravitational wave detection of GW170817 (Abbott et al. 2017), there was an observation of the kilonova light curve produced by the radioactive decay of the neutron-rich nuclei formed during the r-process (Metzger

ggkiss@atomki.hu

et al. 2010; Abbott et al. 2017). Also Sr was directly observed in the kilonova spectrum (Watson et al. 2019). Still there are many open questions concerning the astrophysical site and the nuclear physics involved.

Observations of the oldest stars in our galaxy and in neighbour dwarf galaxies (see e.g., Frebel 2018; Reichert et al. 2020a; Côté et al. 2019) indicate that the r-process occurred already very early, even before neutron star mergers could significantly contribute. This points to rare supernovae, and recent investigations have shown that magneto-rotational supernovae could account for this early r-process contribution (see e.g., Winteler et al. 2012; Nishimura et al. 2017; Mösta et al. 2018; Reichert et al. 2020b). Another hint from observations is that the elements between Sr and Ag may be produced by a separate or additional process to the r-process (Travaglio et al. 2004; Qian & Wasserburg 2000; Montes et al. 2007; Hansen et al. 2014). One possibility to explain these observations is the neutrino-driven ejecta from core-collapse supernovae (Qian & Woosley 1996; Wanajo et al. 2011; Arcones & Montes 2011; Arcones & Bliss 2014).

In neutrino-driven, neutron-rich supernova ejecta, the weak r-process can form the lighter heavy elements between Sr and Ag (see e.g., Bliss et al. 2018). Initially the matter is close to the neutron star and very hot, therefore a nuclear statistical equilibrium (NSE) is established. As matter expands the temperature drops and individual nuclear reactions become important. Bliss et al. (2018) have investigated all possible conditions expected in neutrino-driven, neutron-rich supernova ejecta and identified those where nuclear reactions are important. In the weak r-process, the nucleosynthesis path is determined by (n,γ)-(γ,n) equilibrium and stays close to stability. Consequently, compared to the expansion timescale, β decays are too slow to move matter to higher proton numbers and (α,n) and (p,n) reactions become important as they are faster (Bliss et al. 2017).

Therefore, in order to use observations to understand the astrophysical conditions where lighter heavy elements are produced, one has to reduce the nuclear physics uncertainties of the key reactions. In a broad sensitivity study (Bliss et al. 2020), several (α,n) reactions have been identified as critical because of their impact on the abundances under different astrophysical conditions. These reactions rates are calculated from the cross sections computed with the Hauser-Feshbach statistical model which relies on nuclear physics inputs. Recently, a series of sensitivity calculations were performed to evaluate the theoretical uncertainty of these cross section calculations (Pereira & Montes 2016; Mohr 2016; Bliss et al. 2017). These works identified different α+nucleus optical potential parameter sets (αOMP's) as the main source of uncertainty. The difference between the cross section based on various αOMP's can exceed even an order of magnitude (Pereira & Montes 2016). Therefore, experiments are critical to reduce the uncertainties of the rates. Low energy alpha-induced reaction cross section measurements were frequently used to constrain the parameters of the αOMP's used in astrophysical calculations (Sauerwein et al. 2011; Scholz et al. 2014; Kiss et al. 2015). However, such precise experimental data, reaching sub-Coulomb energies are typically missing for isotopes located at or close to the weak r-process path (Bliss et al. 2017).

TABLE 1
Decay parameters of the reaction product ^{99}Mo and its daughter ^{99}Tc^m, taken from Browne & Tuli (2017); Goswamy et al. (1992).

Residual nucleus	Half-life [h]	Energy [keV]	Relative intensity [%]
^{99}Mo	65.924 ± 0.006	40.58	1.04 ± 0.03
		181.07	6.05 ± 0.12
		366.42	1.20 ± 0.02
		739.50	12.20± 0.02
		777.92	4.31 ± 0.08
^{99}Tc^m	6.0072 ± 0.0009	140.51	89 ± 4

Here we contribute to a more reliable weak r-process calculation by measuring the ^{96}Zr(α,n)^{99}Mo reaction cross section for the first time at energies relevant for the weak r-process nucleosynthesis and by using the precise data to evaluate the αOMP's used in the nucleosynthesis network. This reaction is one of the bottlenecks that sensitively affects the production of nuclei between $44 \leq Z \leq 47$ (Bliss et al. 2020). We demonstrate that reducing the nuclear physics uncertainty to a 30% level is critical and enough to get accurate abundance predictions.

This paper is structured as follows. In Sect. 2, we present our experimental approach. The results including a theoretical analysis are in Sect. 3, and the impact of those on the weak r-process is in Sect. 4. Finally, we provide a short summary and conclusions are given in Sect. 5.

2. EXPERIMENTAL APPROACH

The cross section measurement was carried out at the Institute for Nuclear Research (Atomki) using the activation technique. The targets were prepared by electron beam evaporation of metallic Zr onto 6 μm thick Al foil backing. Similarly to our previous cross section measurements (Korkulu et al. 2018; Kiss et al. 2018), the absolute number of target atoms was determined with the Rutherford Backscattering technique using the Oxford-type Nuclear Microprobe Facility at Atomki (Huszank et al. 2016). The energy and the diameter of the beamspot of the ^{4}He$^+$ beam provided by the Van de Graff accelerator was 2.0 MeV and 2.5 μm, respectively. Two Silicon ion-implanted detectors (50 mm^2 sensitive area and 18 keV energy resolution) were used to measure the yield of the backscattered ions, one of them was placed at a scattering angle of 165° and the other one was set to 135°. Target thicknesses between 1.23 x 10^{18} and 1.54 x 10^{18} Zr atom/cm^2 were found with an uncertainty of typically 5%.

The Zr targets were irradiated with α beams from the MGC cyclotron of Atomki. The energy of the α beam was between $E_{\rm lab}$ = 6.5 MeV and $E_{\rm lab}$ = 13.0 MeV, this energy range was scanned with energy steps of 0.5 MeV - 1.0 MeV. The length of the irradiations varied between $t_{\rm irrad}$ = 6 h to $t_{\rm irrad}$ = 48 h with beam currents of 0.5 - 1.4 μA. Longer irradiations were carried out at lower energies to (partially) compensate the lower cross sections. The number of the impinging α particles was obtained from current measurement. After the beam-defining aperture, the chamber was insulated and secondary electron suppression voltage of −300 V was applied at the entrance of the chamber. From the last beam-defining aperture the whole chamber served as a Faraday cup. The col-

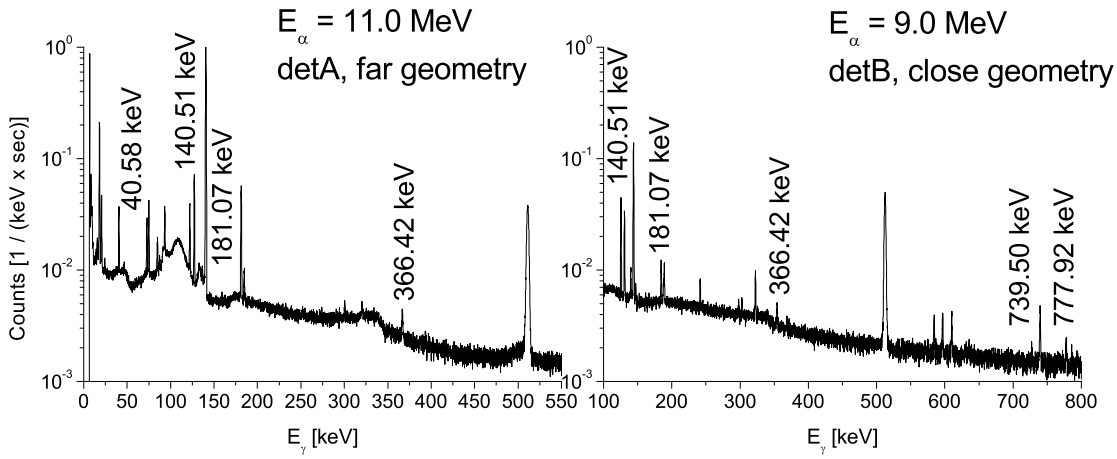

FIG. 1.— γ-ray spectra, measured for one hour, taken on detA, $t_{waiting}$ = 9.5 h after the 11 MeV irradiation (left panel); and on detB, $t_{waiting}$ = 62.6 h after the 9 MeV irradiation (right panel). The peaks used for the analysis are marked.

lected charge was measured with a current integrator, the counts were recorded in multichannel scaling mode, stepping the channel in every minute to take into account the possible changes in the beam current.

The cross sections were measured using the activation technique (Gyürky et al. 2019). The decay parameters of the ^{99}Mo reaction product are summarized in Table 1. The β^- decay of ^{99}Mo is followed by the emission of numerous, relatively intense γ-rays, which were detected by two Germanium detectors: a Low Energy Photon Spectrometer (detA) and a 50% relative efficiency HPGe detector (detB), both equipped with a 4π lead shield. DetA has low laboratory background (about 0.585 1/s in the 50-2000 keV energy region), its resolution is excellent, but with increasing γ-ray energies its detection efficiency decreases sharply. Accordingly, this detector was used to measure the yield of the E_γ = 40.58 keV, E_γ = 140.51 keV (belonging to the daughter isotope ^{99}Tc^m), E_γ = 181.07 keV and E_γ = 366.42 keV transitions. The laboratory background of detB is higher (about 5.071 1/s in the 100-2000 keV energy region), however, its detection efficiency is much higher for the higher energy γ-rays, therefore, this detector was used to measure the yield of the E_γ = 739.50 keV and E_γ = 777.92 keV γ-rays, also. After the irradiations, $t_{\rm waiting} \approx$ 2.0 h waiting time was used in order to let the short-lived, disturbing activities decay. The duration of the γ-countings were two-to-six days in the case of each irradiation and the spectra were saved in every hour. Typical off-line γ spectra, measured with detA (left panel) and detB (right panel), can be seen in Fig. 1. The activity of the samples irradiated at $E_{\rm lab}$ = 8 MeV and higher were measured with both detectors, the resulting cross sections were found to be always consistent. The half-life of the ^{99}Mo is known from large number of experiments with uncertainty less than 0.01% (Stone 2014). The activity of the samples irradiated with alpha beams of $E_{\rm lab}$ = 12 MeV and $E_{\rm lab}$ = 13 MeV energies were measured for more than 2 weeks, the deadtime and relative intensity corrected peak areas were fitted with exponential using the least square method. The resulted half-lives, having χ^2 always below 1.3, are in agreement with the literature value within their uncertainties, which proves that no other γ transitions pollutes the peaks used for cross section determination.

The low yields measured in the present work necessitated the use of short source-to-detector distances for the γ-countings carried out after the irradiation of the Zr targets with alpha beams of $E_{\rm lab}$ = 9.0 MeV and below. The absolute detection efficiency was derived for both detectors using the following procedure: first, using calibrated ^{60}Co, ^{133}Ba, ^{137}Cs, ^{152}Eu, and ^{241}Am sources, the absolute detector efficiency was measured in far geometry: at 15 cm and 21 cm distance from the surface of detA and detB, respectively. Since the calibration sources (especially ^{133}Ba, ^{152}Eu) emit multiple γ-radiations from cascade transitions, in close geometry no direct efficiency measurement was carried out. Instead, in the case of the high energy irradiations (at and above 10 MeV) the yield of the investigated γ-rays was measured both in close and far geometry. Taking into account the time elapsed between the two countings, a conversion factor of the efficiencies between the two geometries could be determined and used henceforward in the analysis.

3. RESULTS AND THEORETICAL ANALYSIS

The measured ^{96}Zr(α,n)^{99}Mo cross section values are listed in Table 2. The effective center-of-mass energy in the second column takes into account the energy loss of the beam in the target. The quoted uncertainty in the $E_{\rm c.m.}$ values corresponds to the energy stability of the α-beam and to the uncertainty of the energy loss in the target, which was calculated using the SRIM code (Ziegler et al. 2008). The activity of several targets were measured using both detA and detB, in these cases the cross sections were derived from the averaged results weighted by the statistical uncertainty of the measured values. The uncertainty of the cross sections is the quadratic sum of the following partial errors: detection efficiency (5%), far-to-close detection efficiency correction factor ($\leq$ 2%), number of target atoms (5%), current measurement (3%), uncertainty of decay parameters ($\leq$ 4%) and counting statistics ($\leq$ 15.3%). The new data are shown in Fig. 2, and a comparison to theoretical predictions is

TABLE 2
MEASURED CROSS SECTIONS OF THE ^{96}ZR(α,N)^{99}MO REACTION. THE LAST FIVE ROWS SHOW THE AVERAGE RESULTS (WEIGHTED BY THE STATISTICAL UNCERTAINTIES) OF THE MEASUREMENTS CARRIED OUT AT THE SAME ENERGY.

$E_{\mathrm{c.m.}}$ [MeV]	Cross section [mbarn]
6.22 ± 0.02	(2.49 ± 0.52) · 10^{-4}
6.22 ± 0.02	(2.54 ± 0.48) · 10^{-4}
6.67 ± 0.02	(1.65 ± 0.22) · 10^{-3}
6.66 ± 0.02	(1.64 ± 0.19) · 10^{-3}
7.19 ± 0.02	(1.32 ± 0.13) · 10^{-2}
7.18 ± 0.02	(1.42 ± 0.11) · 10^{-2}
7.66 ± 0.02	(6.29 ± 0.62) · 10^{-2}
7.66 ± 0.02	(6.29 ± 0.49) · 10^{-2}
8.14 ± 0.03	(2.14 ± 0.17) · 10^{-1}
8.62 ± 0.03	(7.90 ± 0.67) · 10^{-1}
9.11 ± 0.03	(2.48 ± 0.19) · 10^{0}
9.58 ± 0.03	(5.27 ± 0.51) · 10^{0}
9.59 ± 0.03	(5.58 ± 0.43) · 10^{0}
10.55 ± 0.03	(3.48 ± 0.29) · 10^{1}
11.51 ± 0.04	(8.38 ± 0.71) · 10^{1}
12.47 ± 0.04	(1.33 ± 0.12) · 10^{2}
12.47 ± 0.04	(1.36 ± 0.10) · 10^{2}
6.22 ± 0.02	(2.52 ± 0.48) · 10^{-4}
6.66 ± 0.02	(1.64 ± 0.18) · 10^{-3}
7.18 ± 0.02	(1.38 ± 0.11) · 10^{-2}
7.66 ± 0.02	(6.29 ± 0.49) · 10^{-2}
9.59 ± 0.03	(5.47 ± 0.41) · 10^{0}
12.47 ± 0.04	(1.35 ± 0.10) · 10^{2}

made.

The ^{96}Zr(α,n)^{99}Mo reaction was already studied in several works (Chowdhury et al. 1995; Pupillo et al. 2015; Hagiwara et al. 2018; Murata et al. 2019). However, because the literature data do not reach the lowest energies, and because of the significant scatter of the literature data below 11 MeV, the further analysis is restricted to our new experimental results.

The new experimental data for the ^{96}Zr(α,n)^{99}Mo reaction have been analyzed in the statistical model (SM), complemented by the recently suggested pure barrier transmission model (PTBM) (Mohr et al. 2020). In a schematic notation, the cross section of an α-induced (α,X) reaction is given by

$$\sigma(\alpha, X) \sim \frac{T_{\alpha,0} T_X}{\sum_{T_i}} = T_{\alpha,0} \times b_X \qquad (1)$$

with the transmission coefficients $T_{\alpha,0}$ of the incoming α-particle, T_i for the outgoing particles ($i = \gamma, p, n, \alpha, 2n$, etc.), and the branching ratio $b_X = T_X / \sum_i T_i$ for the branching into the X channel. Usually, the transmissions T_i are calculated from optical model potentials for the particle channels and from the γ-ray strength function for the (α,γ) capture channel. For further details, see e.g. Rauscher & Thielemann (2000); Rauscher (2011).

For the ^{96}Zr(α,n)^{99}Mo reaction in the energy range under study (see Fig. 2) the neutron channel is dominating because the proton channel is closed or suppressed by the Coulomb barrier and the γ-channel is typically much weaker than the neutron channel. Thus, the branching ratio to the neutron channel is $b_n \approx 1$, and the (α,n) cross section is almost identical to the total α-induced reaction cross section σ_{reac}. From Eq. (1) it can be seen that the (α,n) cross section is essentially defined by the transmission $T_{\alpha,0}$ which in turn depends only on the chosen αOMP. Other ingredients of the statistical model affect the branching ratios b_X, but have only minor influence on the (α,n) cross section because of $b_n \approx 1$. For completeness we note that below the (α,n) threshold at 5.1 MeV, we find $b_\gamma \approx 1$, and the (α,γ) cross section approaches the total cross section σ_{reac}.

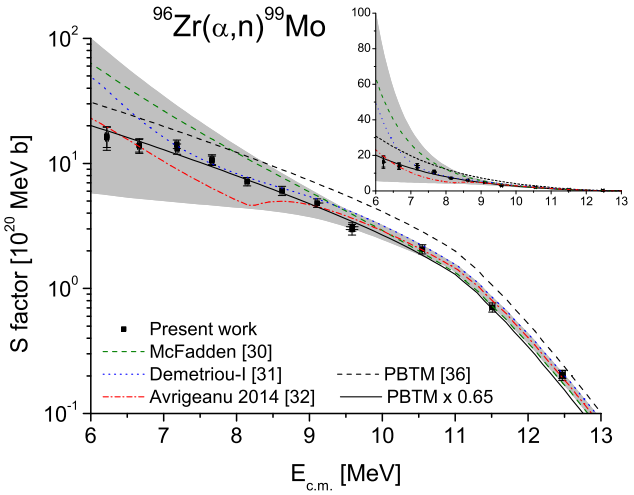

FIG. 2.— Comparison of experimental and theoretical astrophysical S-factors of ^{96}Zr(α,n)^{99}Mo reaction as a function of the energy (the inset shows the same data on linear scale). Excellent agreement with $\chi^2/N < 1$ is only obtained for the PBTM calculation, scaled by a factor of 0.65 (full line). The wide range of TALYS predictions is indicated by the grey-shaded area. Further discussion see text.

It is obvious from Fig. 2 that predictions of the (α,n) cross sections in the SM vary over more than one order of magnitude at the lowest energies whereas at energies above 10 MeV most predictions agree nicely. For better readability of Fig. 2, we restrict ourselves to the presentation of the widely used αOMP's by McFadden & Satchler (1966), Demetriou et al. (2002), and Avrigeanu et al. (2014); the latter is the default αOMP in TALYS (which is a widely used nuclear reaction code; the calculations shown in Fig. 2 were carried out using version 1.9).

The reason for the wide range of predictions was identified and discussed in Mohr et al. (2020). The usual SM calculations show a dramatic sensitivity to the tail of the imaginary potential. To avoid this sensitivity, an alternative approach was suggested in Mohr et al. (2020) to use the PBTM model for the calculation of the total reaction cross section σ_{reac}. The Supplement of Mohr et al. (2020) provides the new ATOMKI-V2 αOMP which reproduces measured (α,n) cross sections over a wide range of masses and energies with deviations below a factor of two. This holds also for the present ^{96}Zr(α,n)^{99}Mo reaction (see Fig. 2). However, there is a slight overestimation of the experimental results over the full energy range under study (dotted line in Fig. 2). Therefore the calculation from the ATOMKI-V2 potential was scaled by a factor of 0.65 to obtain best agreement with the new experimental data. These scaled cross sections were used to calculate the astrophysical reaction rate $N_A\langle\sigma v\rangle$ (see below).

Although the scaling factor of 0.65 is within the estimated uncertainty of the new approach of Mohr et al.

(2020), a brief discussion of this factor is appropriate:

(*i*) Technically, the ATOMKI-V2 potential is a complex αOMP which approximates the calculations in the PBTM with small deviations. In the present case, the ATOMKI-V2 calculation of the total cross section $\sigma_{\rm reac}$ is about 10% higher than the underlying PBTM calculation.

(*ii*) The ATOMKI-V2 potential distinguishes between semi-magic and non-magic target nuclei; the latter (like ^{96}Zr in this work) require a deeper potential with volume integrals of $J_R = 371$ MeV fm^3 whereas the semi-magic targets are characterized by a lower $J_R = 342.4$ MeV fm^3. Depending on energy, the lower J_R for semi-magic targets increases the effective barrier and thus reduces $\sigma_{\rm reac}$ by about $15-25$%. An analysis of ^{96}Zr(α,α)^{96}Zr elastic scattering at 35 MeV (Lund et al. 1995; Lahanas et al. 1986) requires volume integrals around $J_R \approx 350$ MeV fm^3, thus indicating that ^{96}Zr behaves more like a semi-magic nucleus. As a consequence, the usage of the global value $J_R = 371$ MeV fm^3 instead of the locally optimized $J_R \approx 350$ MeV fm^3 leads to an overestimation of $\sigma_{\rm reac}$ by about $10-20$%.

Combining the above arguments (*i*) and (*ii*) provides a reasonable explanation for the obtained scaling factor of 0.65 for the ATOMKI-V2 result using the global $J_R = 371$ MeV fm^3 for non-magic target nuclei.

Finally, the agreement of the scaled ATOMKI-V2 calculation with the experimental data is excellent with χ^2 per point of about 0.6 whereas calculations with the different αOMPs within TALYS show a different energy dependence (see Fig. 2) and cannot reach $\chi^2/N < 3$ (even with arbitrary scaling factors). The ATOMKI-V2 approach, scaled by the factor of 0.65, is thus the preferred option for the calculation of the astrophysical reaction rate $N_A\langle\sigma v\rangle$.

The lowest experimental data point at about 6.2 MeV is located only 1.1 MeV above the (α,n) threshold at 5.1 MeV. The astrophysical reaction rate $N_A\langle\sigma v\rangle$ results from the folding of a Maxwell-Boltzmann velocity distribution with the energy-dependent cross section $\sigma(E)$. At higher temperatures, the folding integral is essentially determined by the new experimental data. At lower temperatures, the calculation of the rate has to rely on the calculated cross section between the threshold at 5.1 MeV and the lowest data point at 6.2 MeV. Because of the excellent reproduction of the energy dependence of the (α,n) cross section we estimate an overall uncertainty of less than 30% for all temperatures. The obtained reaction rates are listed in Table 3. Compared to previously recommended rates, e.g. from REACLIB (REACLIB 2015; Cyburt et al. 2010), STARLIB (STARLIB 2017; Sallaska et al. 2013), or NON-SMOKER (Rauscher & Thielemann 2000) which vary by more than one order of magnitude, the uncertainty of the present recommended rate is reduced significantly to about 30%.

4. IMPACT ON WEAK R-PROCESS

We investigate the impact of the new experimental data on the nucleosynthesis of lighter heavy elements in neutron-rich supernova ejecta. We use astrophysical trajectories based on the neutrino-driven wind model of Bliss et al. (2018). Each trajectory corresponds to a combination of astrophysical parameters which are expected for neutrino-driven winds. The 36 trajectories under consideration (see Table I of Bliss et al. (2020)) cover electron fractions between 0.40 and 0.49, entropies between 32 and 175 $k_{\rm B}$ per nucleon, and expansion timescales from 9.7 to 63.8 ms. In that work, the authors identified the conditions for which (α,n) reactions have a significant impact on the final abundances. Under such conditions, Bliss et al. (2020) used 36 trajectories to identify key (α,n) reactions. The reaction ^{96}Zr(α,n)^{99}Mo is in their list of key reactions. Our nucleosynthesis calculations are performed with the WinNet reaction network (Winteler et al. 2012). Reaction rates are taken from the JINA REACLIBV2.0 (REACLIB 2015; Cyburt et al. 2010) library except for (α,n) reactions for which TALYS 1.6 with the GAOP αOMP was used (for more details see Bliss et al. (2018, 2020)). Replacing the ^{96}Zr(α,n)^{99}Mo reaction rate with the values from Tab. 3 results in a reduction of the final abundances by more than 10% in 17 and by more than 20% in 6 of the 36 trajectories. More importantly, the reduced reaction-rate uncertainty leads to a significant improvement in the accuracy of the nucleosynthesis predictions. Following Bliss et al. (2020) we estimate the uncertainty of the ^{96}Zr(α,n)^{99}Mo reaction rate calculated with the GAOP with the factors 0.1 and 10 and the uncertainty of the updated (PBTM) reaction rate with 30% (see Sect. 3).

TABLE 3
RECOMMENDED ASTROPHYSICAL REACTION RATE $N_A\langle\sigma v\rangle$ OF THE ^{96}ZR(α,N)^{99}MO REACTION.

T_9	$N_A\langle\sigma v\rangle$ (cm^3 s^{-1} mole^{-1})
1.0	2.09×10^{-25}
1.5	1.36×10^{-16}
2.0	5.44×10^{-12}
2.5	5.01×10^{-09}
3.0	7.11×10^{-07}
4.0	7.03×10^{-04}
5.0	4.44×10^{-02}

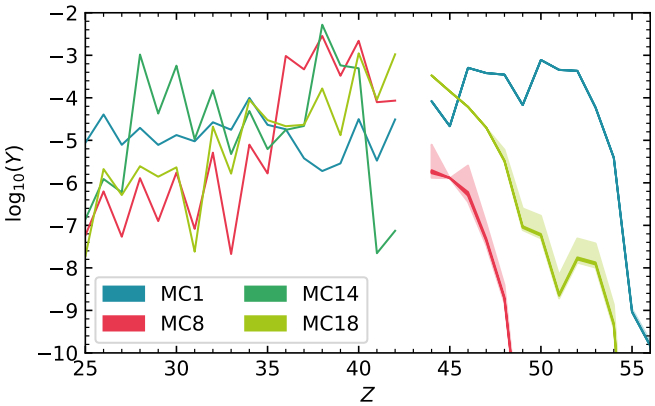

FIG. 3.— Elemental abundances for four trajectories from Bliss et al. (2020). The lightly shaded regions correspond to the uncertainties due to variations of the previously used ^{96}Zr(α,n)^{99}Mo reaction rate by factors 10 and 0.1. The solid bands correspond to the uncertainties due to variations of the updated reaction rate by 30%.

In Fig. 3, we present the impact of the reduced uncertainty of the new experimentally based reaction rate for four representative trajectories from Bliss et al. (2020). Changes of the final abundances resulting from the vari-

ation of the GAOP and PBTM ^{96}Zr(α,n)^{99}Mo reaction rate are represented by the shaded and solid bands, respectively (note that the figure shows solid colored bands and not thick lines). If large amounts of elements heavier than Tc are produced (e.g., trajectory MC1 in Fig. 3), the abundances are not sensitive to ^{96}Zr(α,n)^{99}Mo, because the nucleosynthesis path runs along more neutron-rich nuclei. Trajectories that do not produce any elements beyond Mo (e.g., trajectory MC14 in Fig. 3) are not sensitive either. For roughly half of the 36 trajectories, the variation of the previously used ^{96}Zr(α,n)^{99}Mo reaction rate leads to a significant spread (up to a factor of 6 between the lower and upper estimate) in the elemental abundances between Ru and Xe (e.g., trajectories MC8 and MC18 in Fig. 3). In all of these trajectories, the lower uncertainty of the PBTM reaction rate leads to greatly improved accuracy in the final abundances. In Fig. 4, we show the abundances for trajectory MC8 in detail. The orange and blue bands represent the uncertainty as estimated for the GAOP and the PBTM reaction rate, respectively. The dashed and dotted lines in the upper panel show the abundance pattern calculated with upper and lower uncertainty estimation of the GAOP reaction rate, respectively. In the bottom panel, we show the uncertainty for each element relative to the abundances calculated with the unvaried GAOP reaction rate, $Y_{\rm base}$. Since ^{96}Zr(α,n)^{99}Mo forms a bottleneck for this trajectory, an increase of the reaction rate results in higher abundances of elements heavier than Tc. The PBTM reaction rate is slightly lower than the GAOP reaction rate and thus the abundances are slightly lower than $Y_{\rm base}$. An exception is the abundance of Rhodium which is not sensible to ^{96}Zr(α,n)^{99}Mo. Rhodium possesses only one stable isotope, ^{103}Rh, which in all trajectories is mainly produced by the decay of ^{103}Nb. Its abundance is therefore not correlated to ^{96}Zr(α,n)^{99}Mo.

In summary, the reduction of the uncertainty to 30% is sufficient to get very accurate abundances. This accuracy is crucial for comparing theoretical nucleosynthesis calculations with observations. A similar reduction of the uncertainties for other reactions is necessary to reliably compare nucleosynthesis calculations with observations. The PBTM should allow for such a reduction of uncertainties; a detailed investigation is in preparation. This will allow to constrain the astrophysical site of the weak r-process and to further understand core-collapse supernovae and the origin of the lighter heavy elements.

5. SUMMARY AND CONCLUSIONS

In a recent sensitivity study of the weak r-process (Bliss et al. 2020), the ^{96}Zr(α,n)^{99}Mo reaction was identified as a bottleneck for the nucleosynthesis between ruthenium and cadmium, i.e. for nuclei with $Z = 44 - 48$. The typically assumed uncertainties of (α,n) reaction rates of a factor of 10 lead to significant uncertainties for the nucleosynthetic yields in the weak r-process of about a factor of 5; thus the nuclear uncertainties prevent any robust astrophysical conclusion.

In the present study, the cross section of the ^{96}Zr(α,n)^{99}Mo reaction has been measured for the first time from energies close above the reaction threshold at 5.1 MeV up to about 12.5 MeV, thus covering the region relevant for the weak r-process. The chosen activation technique provides the total production cross section of

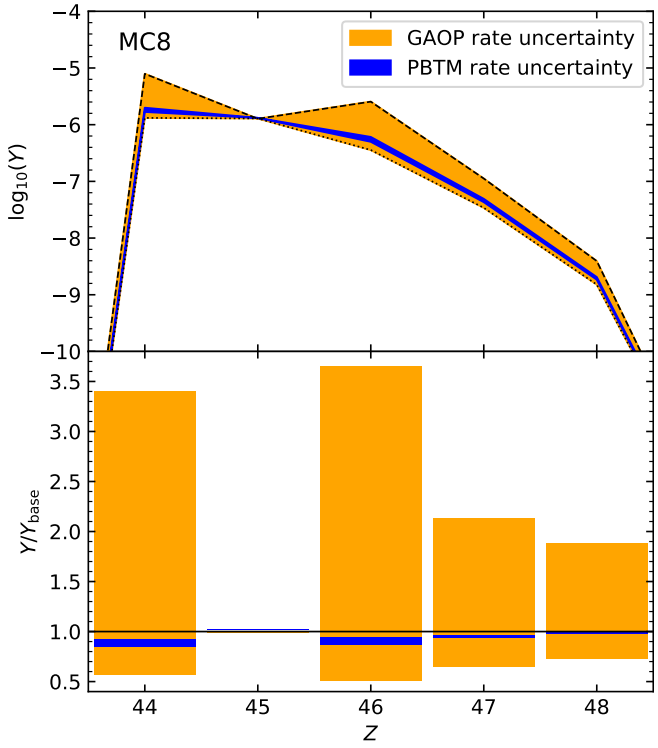

FIG. 4.— Influence of the ^{96}Zr(α,n)^{99}Mo rate on trajectory MC8. Upper panel: Abundance uncertainty of elements between Ru and Cd. The orange and blue bands correspond to the previously used (GAOP) and the updated (PBTM) reaction rate, respectively. The dashed and dotted lines show the abundance pattern calculated with upper and lower uncertainty estimation of the GAOP rate, respectively. Lower panel: Abundance uncertainties relative to the unvaried GAOP reaction rate, $Y_{\rm base}$, in a linear scale.

^{99}Mo which is an excellent basis for the calculation of the astrophysical production rate of molybdenum from ^{96}Zr by α-induced reactions. The high precision experimental data have been analyzed in the statistical model, using global αOMP's and complemented by the recently suggested PBTM model. It was found that the PBTM model — re-scaled by 0.65 — excellently reproduces the new experimental data. The best-fit from the scaled PBTM was used to calculate the astrophysical reaction rates as a function of temperature. For the full temperature range of the weak r-process, the uncertainty of the reaction rate could be drastically reduced from the usually assumed factor of 10 down to about 30%.

A repetition of the nucleosynthesis calculations of Bliss et al. (2020) with the new experimentally based ^{96}Zr(α,n)^{99}Mo reaction rate and its small uncertainties leads to very well-constrained nucleosynthesis yields for the $Z = 44 - 48$ range. As the PBTM is typically able to predict α-induced reaction cross sections with uncertainties below a factor of two, a re-calculation of the full weak r-process network with updated rates from the PBTM will lead to more robust nucleosynthesis yields which in turn should enable a major step towards stringent constraints for the astrophysical conditions and the site of the weak r-process.

The authors thank Julia Bliss, Fernando Montes, Jorge Pereira, and Zs. Fülöp for valuable discussions. This

work was supported by NKFIH (NN128072, K120666, K134197), and by the ÚNKP-20-5-DE-2 New National Excellence Program of the Ministry of Human Capacities of Hungary. G. G. Kiss acknowledges support from the János Bolyai research fellowship of the Hungarian Academy of Sciences. MJ and AA were supported by the ERC Starting Grant EUROPIUM-677912, Deutsche Forschungsgemeinschaft through SFB 1245, and Helmholtz Forschungsakademie Hessen fr FAIR. This work has benefited from the COST Action ChETEC (CA16117) supported by COST (European Cooperation in Science and Technology). The nucleosynthesis computations were performed on the Lichtenberg High Performance Computer (TU Darmstadt).

REFERENCES

Abbott, B. P., Abbott, R., Abbott, T. D., et al. 2017, Phys. Rev. Lett., 119, 161101
Arcones, A., & Bliss, J. 2014, J. Phys. G, 41, 044005
Arcones, A., & Montes, F. 2011, ApJ, 731, 5
Arcones, A., & Thielemann, F. K. 2013, Journal of Physics G Nuclear Physics, 40, 013201
Avrigeanu, V., Avrigeanu, M., & Mănăilescu, C. 2014, Phys. Rev. C, 90, 044612
Bliss, J., Arcones, A., Montes, F., & Pereira, J. 2017, J. Phys. G, 44, 054003
—. 2020, Phys. Rev. C, 101, 055807
Bliss, J., Witt, M., Arcones, A., Montes, F., & Pereira, J. 2018, ApJ, 855, 135
Browne, E., & Tuli, J. K. 2017, Nucl. Data Sheets, 145, 25
Chowdhury, D. P., Pal, S., Saha, S. K., & Gangadharan, S. 1995, Nucl. Instr. Meth in Phys. Res. B, 103, 261
Côté, B., Eichler, M., Arcones, A., et al. 2019, ApJ, 875, 106
Cyburt, R. H., Amthor, A. M., Ferguson, R., et al. 2010, ApJS, 189, 240
Demetriou, P., Grama, C., & Goriely, S. 2002, Nucl. Phys. A, 707, 253
Frebel, A. 2018, Annual Review of Nuclear and Particle Science, 68, 237
Goswamy, J., Chand, B., Mehta, D., Singh, N., & Trehan, P. 1992, Int. J. Radiat. Appl. Instrum. Part A, 43, 1467
Gyürky, G., Fülöp, Z., Käppeler, F., Kiss, G. G., & Wallner, A. 2019, Eur. Phys. J. A, 55, 41
Hagiwara, M., Yashima, H., Sanami, T., & Yonai, S. 2018, J. Radioanal. Nucl. Chem., 318, 569
Hansen, C. J., Montes, F., & Arcones, A. 2014, ApJ, 797, 123
Huszank, R., Csedreki, L., Kertész, Z., & Török, Z. 2016, J. Radioanal. Nucl. Chem., 307, 341
Kiss, G. G., Szücs, T., Mohr, P., et al. 2018, Phys. Rev. C, 97, 055803
Kiss, G. G., Szücs, T., Rauscher, T., et al. 2015, J. Phys. G, 42, 055103
Korkulu, Z., Özkan, N., Kiss, G. G., et al. 2018, Phys. Rev. C, 97, 045803
Lahanas, M., Rychel, D., Singh, P., et al. 1986, Nucl. Phys. A, 455, 399
Lund, B. J., Bateman, N. P. T., Utku, S., Horen, D. J., & Satchler, G. R. 1995, Phys. Rev. C, 51, 635
McFadden, L., & Satchler, G. R. 1966, Nucl. Phys., 84, 177
Metzger, B. D., Martínez-Pinedo, G., Darbha, S., et al. 2010, MNRAS, 406, 2650
Mohr, P. 2016, Phys. Rev. C, 94, 035801
Mohr, P., Fülöp, Z., Gyürky, G., Kiss, G. G., & Szücs, T. 2020, Phys. Rev. Lett., 124, 252701
Montes, F., Beers, T. C., Cowan, J. J., et al. 2007, ApJ, 671, 1685
Mösta, P., Roberts, L. F., Halevi, G., et al. 2018, ApJ, 864, 171
Murata, T., Aikawa, M., Saito, M., et al. 2019, Nucl. Instr. Meth in Phys. Res. B, 458, 21
Nishimura, N., Sawai, H., Takiwaki, T., Yamada, S., & Thielemann, F.-K. 2017, ApJ, 836, L21
Pereira, J., & Montes, F. 2016, Phys. Rev. C, 93, 034611
Pupillo, G., Esposito, J., Haddad, F., Michel, N., & Gambaccini, M. 2015, J. Radioanal. Nucl. Chem., 305, 73
Qian, Y.-Z., & Wasserburg, G. J. 2000, Phys. Rep., 333, 77
Qian, Y.-Z., & Woosley, S. E. 1996, ApJ, 471, 331
Rauscher, T. 2011, Int. J. Mod. Phys. E, 20, 1071
Rauscher, T., & Thielemann, F.-K. 2000, At. Data Nucl. Data Tables, 75, 1
REACLIB. 2015, Reaction rate database REACLIB, version 2.0, https://groups.nscl.msu.edu/jina/reaclib/db/
Reichert, M., Hansen, C. J., Hanke, M., et al. 2020a, arXiv e-prints, arXiv:2004.01195
Reichert, M., Obergaulinger, M., Eichler, M., Aloy, M. Á., & Arcones, A. 2020b, in preparation
Sallaska, A. L., Iliadis, C., Champange, A. E., et al. 2013, ApJS, 207, 18
Sauerwein, A., Becker, H. W., Dombrowski, H., et al. 2011, Phys. Rev. C, 84, 045808
Scholz, P., Endres, A., Hennig, A., et al. 2014, Phys. Rev. C, 90, 065807
STARLIB. 2017, Reaction rate database STARLIB, V6.5, 09-06-2017, https://starlib.github.io/Rate-Library/
Stone, N. J. 2014, Rept INDC(NSD)-0658
Travaglio, C., Gallino, R., Arnone, E., et al. 2004, ApJ, 601, 864
Wanajo, S., Janka, H.-T., & Müller, B. 2011, ApJ, 726, L15
Watson, D., Hansen, C. J., Selsing, J., et al. 2019, Nature, 574, 497
Winteler, C., Käppeli, R., Perego, A., et al. 2012, ApJ, 750, L22
Ziegler, J. F., Ziegler, M. D., & Biersack, J. P. 2008, Code SRIM, Version 2008.4, http://www.srim.org/SRIM/SRIMLEGL.htm